

1 Million Intrinsic Q-Factor Microring Resonators From PVD Aluminum Nitride on SiO₂-on-Si Substrate

Amy S. K. Tong,^{1,*} Wing Wai Chung,¹ Charmaine Goh,¹ Landobasa Y. M. Tobing,¹ Leh Woon Lim,¹ Yuriy A. Akimov,² Zhan Jiang Quek,¹ Aravind P. Anthur,³ Jia Sheng Goh,¹ Huamao Lin,¹ Navab Singh,¹ Qingxin Zhang,¹ Doris K. T. Ng,^{1,†}

¹Institute of Microelectronics (IME), Agency for Science, Technology and Research (A*STAR),
2 Fusionopolis Way, Innovis #08-02 Singapore 138634, Republic of Singapore

²Institute of High Performance Computing (IHPC), Agency for Science, Technology and Research (A*STAR),
1 Fusionopolis Way, Connexis #16-16 Singapore 138632, Republic of Singapore

³Institute of Materials Research and Engineering (IMRE), Agency for Science, Technology and Research (A*STAR),
2 Fusionopolis Way, Innovis #08-03, Singapore 138634, Republic of Singapore

* amy_tong@ime.a-star.edu.sg and [†]doris_ng@ime.a-star.edu.sg

Abstract: We present PVD AlN microring resonators on SiO₂-on-Si substrate with intrinsic Q-factor >1 million at C-band. To the best of our knowledge, this is the highest intrinsic Q-factor reported for PVD AlN on SiO₂-on-Si substrate. © 2024 The Author(s)

1. Introduction

Aluminum nitride (AlN) is a strong candidate for wideband frequency comb generation owing to its large bandgap (6.2 eV) and suppressed two-photon absorption. Its high thermal conductivity (~285 W/mK) allows AlN devices to handle high power, which is advantageous for nonlinear optics applications that generally require high power. Importantly, thin film deposition of AlN on 8- [1] and 12-inch wafers and its CMOS compatibility makes it feasible for integration with other passive devices realized by silicon photonics. In addition, the multifaceted properties of AlN allow for wide range of applications from photonics to gas sensing [2]. Deposition of AlN has been mainly explored by two methods, namely the physical vapor deposition (PVD) [3-6] sputtering and metal-organic chemical vapor deposition (MOCVD) [7-10]. The latter has been shown to realize highly crystalline AlN film, with X-ray diffraction (XRD) rocking curve showing c-axis full-width-at-half-maximum (FWHM) of ~0.013° [11]. However, such a c-axis orientated AlN film is typically grown on sapphire substrate, which presents challenges in the subsequent facet cutting due to hardness of the sapphire glass. In addition, sapphire substrates are generally more expensive compared to silicon, and cannot be readily integrated into silicon photonic process. On the other hand, depositing by PVD method may address the challenges faced by the MOCVD and sapphire substrate, as the AlN film can be deposited on silicon substrate, thus enabling the integration with other CMOS-compatible process. PVD-deposited AlN on Si has been demonstrated to have c-axis XRD rocking curve of 2° or smaller [9]. However, despite its lower crystalline quality than those grown by MOCVD, it is desirable to have a CMOS-compatible AlN deposition process as it allows low temperature process, scalable, and monolithic integration with diverse active and passive photonic functions already existing in Si photonics.

In this paper, we demonstrate the fabrication and characterization of AlN-based waveguide and microring devices exhibiting waveguide loss in the sub-1 dB/cm range and intrinsic quality (Q) factor of more than 1 million. The material characteristics of the AlN thin film, deposited by PVD on SiO₂-on-Si substrate, is systematically studied and presented, from its crystalline structure (XRD, TEM), refractive index (ellipsometry), to its surface roughness (AFM). To the best of our knowledge, this is the highest Q-factor reported at C-band for PVD-deposited AlN on SiO₂-on-Si substrate.

2. Material properties of AlN on SiO₂-on-Si film

300 nm thick AlN films were deposited by PVD on 8-inch SiO₂-on-Si substrates at deposition temperature of 200°C, where the SiO₂ film on the Si substrate was thermally grown with thickness of ~5 μm. After deposition, the AlN films underwent annealing treatment before their material properties were characterized.

Fig. 1a shows the refractive index (*n*) and extinction coefficient (*k*) of the AlN film, extracted from ellipsometry measurements for 300 to 2350 nm wavelength range. The (*n*, *k*) spectra show characteristics of a Cauchy-like transparent dielectric material, with *n* ranging from ~2.04 (at λ = 2350 nm) to ~2.23 (at λ = 300 nm), and negligible extinction coefficient (*k*~0) within 300 to 2350 nm wavelength range. The XRD scan reveals crystalline AlN at c-axis (0002) orientation occurring at ~35.8° (Fig. 1b), with its rocking curve measuring FWHM of ~2.029° (Fig. 1c). The root mean square (rms) surface roughness of the AlN films (over 1 μm x 1 μm scan window) is measured to be ~2.82 nm (Fig. 1d). The AFM scan reveals circular grains in the film morphology, which is attributed to the columnar structures of the AlN. This is verified by the cross-sectional transmission electron microscopy (TEM) image of the

AlN on SiO₂ (see Fig. 1e), where the columnar structures can be clearly observed. Furthermore, the electron diffraction pattern (inset of Fig. 1e) reveals crystalline structure with (0002) and (01-10) orientations, confirming the XRD scan in Fig. 1b.

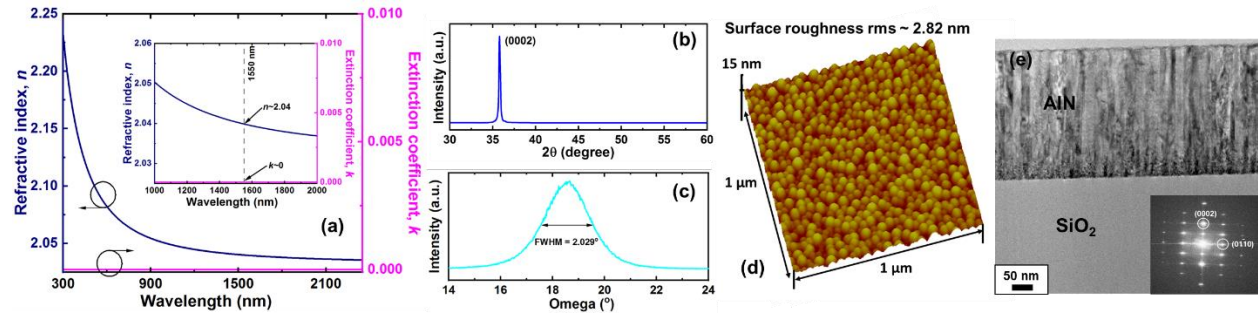


Fig. 1. (a) Ellipsometry measurement of our PVD AlN film's n and k for wavelength between 300 - 2300 nm. Inset shows that at 1550 nm, $n \sim 2.04$ and $k \sim 0$. (b) 2-Theta XRD scans from 30° - 60° measure crystalline AlN at $\sim 35.8^\circ$ indexed at (0002). (c) Rocking curve XRD shows AlN with FWHM of $\sim 2.029^\circ$. (d) AFM measurement over scan window ($1 \mu\text{m} \times 1 \mu\text{m}$) on AlN exhibits multiple columnar structures with a surface roughness rms of ~ 2.82 nm. (e) Cross-sectional TEM image of AlN shows columnar structure of PVD AlN. Inset shows the electron diffraction of AlN.

3. AlN Photonics Devices on SiO₂-on-Si

Owing to the similarity of refractive index values of AlN with that of the silicon nitride (SiN), the thickness of the optical waveguide is chosen to be similar to the baseline thickness for the SiN photonics (i.e. ~ 400 nm). As with our material study, 400 nm thick AlN was deposited by PVD at 200°C deposition temperature on $5 \mu\text{m}$ thick thermal oxide on Si substrate. Afterwards, SiO₂ was deposited as hard mask material, followed by patterning of the photonic structures by 248 nm DUV lithography tool. Subsequently, the AlN film was dry etched and SiO₂ was deposited as upper cladding layer for the AlN waveguides. Finally, the AlN devices were annealed under optimized conditions for improved (0002) orientation. The cross-sectional TEM image of the fabricated AlN waveguide is shown in Fig. 2a.

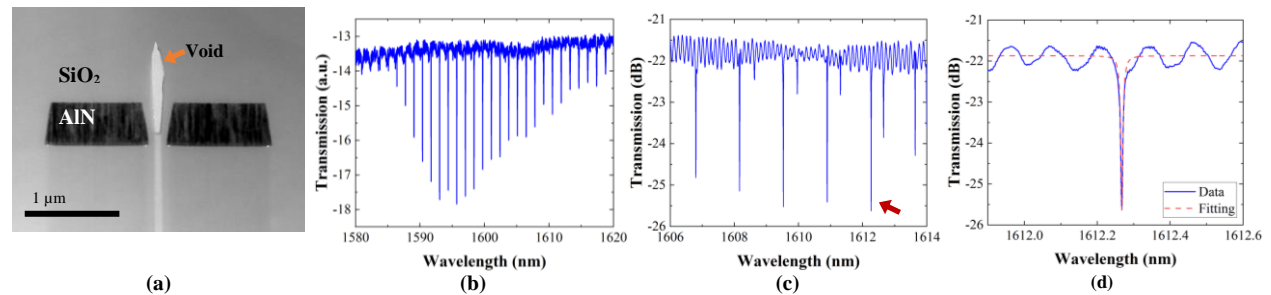


Fig. 2. (a) A cross-section TEM image of the AlN waveguide cladded in SiO₂, and transmission spectrum of 100 μm radius AlN microring resonator (b) with ring width of 890 nm and gap between bus waveguide and microring resonator of 400 nm, (c) with width of 790 nm and gap of 400 nm, and (d) zoom-in spectrum of measured (blue) and fitted (red) resonance peak at 1612 nm with intrinsic Q-factor of 1.03×10^6 .

For self-consistent characterization of the photonic devices, both waveguides and microring devices were fabricated on the same chip. The propagation loss was deduced from the cutback method, and then employed to verify the intrinsic Q -factor of the microring resonators. The light from tunable laser (C-band) was launched into the waveguide facet through a polarization-maintaining fiber, and couples to the AlN waveguide through edge couplers. The output light was then collected from the end-facet with another polarization-maintaining fiber, into the power meter synchronized with the wavelength of the tunable laser where transmission spectrum was obtained. The cutback measurement showed waveguide losses (at $\lambda = 1550$ nm) of ~ 1.61 dB/cm and ~ 0.37 dB/cm for TE and TM modes, respectively. The lower propagation loss for the TM mode (y -polarized mode field) is likely attributed to the dominant evanescent field along the vertical direction, which translates to the reduced evanescent fields along the horizontal direction which interacts with the waveguide sidewall roughness. This contrasts with the TE mode which exhibits stronger evanescent fields along the horizontal direction, which gives rise to higher scattering loss due to spatial mode overlap with the sidewall roughness. We note that there also exists substrate leakage loss for the TM mode, as is common for the TM mode in the silicon-on-insulator (SOI) waveguide. However, this substrate leakage loss is negligible because the lower cladding thickness in our case is much thicker (i.e. $5 \mu\text{m}$) than the typical $2 \mu\text{m}$ buried oxide in SOI waveguide. Another likely cause is the columnar structure of the AlN material, which leads to the anisotropic refractive index, causing the vertical confinement to be intrinsically stronger than the horizontal.

The microring resonators were fabricated with different waveguide width and gap spacings. Fig. 2b shows the transmission spectrum of a microring coupled to a single waveguide, with gap spacing of 400 nm and waveguide width of 890 nm. The critical coupling condition can be observed when the transmission contrast is the largest (around 1595 nm), with the wavelength band at the right and left side of the critical coupling denoted as the over- and under-coupling conditions, respectively. The transmission of microring resonator with 790 nm waveguide width and 400 nm gap spacing is shown in Fig. 2c. The microring resonator is characterized by fitting the transmission response with $T = (T_{\text{res}}(\Delta\omega/2)^2 + (\omega - \omega_{\text{res}})^2) / ((\Delta\omega/2)^2 + (\omega - \omega_{\text{res}})^2)$, where T_{res} is the transmission at the resonance, $\Delta\omega$ is the fitted FWHM of the resonance linewidth, and ω_{res} is the resonance frequency. The loaded ($Q_{\text{load}} = \omega_{\text{res}} / \Delta\omega$) and intrinsic (Q_{int}) Q-factors were then related by $Q_{\text{int}} = 2Q_{\text{load}} / (1 \pm \sqrt{T_{\text{res}}})$, and the deduced Q_{int} was verified by relating it to the propagation loss α , $Q_{\text{int}} = 2\pi n_g / (\lambda_{\text{res}} \alpha)$, with n_g as the group index of the AlN waveguide at resonance wavelength λ_{res} . One exemplary fitting for microring with 790 nm waveguide width is shown in Fig. 2d, where $Q_{\text{int}} \sim 1.03 \times 10^6$ was deduced for TM mode at $\lambda = 1612$ nm. This propagation loss of 0.32 dB/cm is consistent with the propagation loss measured independently from the cutback method, which predicts $Q_{\text{int}} \sim 1$ million.

4. Conclusions

In summary, we demonstrate for the first time PVD AlN on SiO₂-on-Si microring resonators with high Q-factor of >1 million in the C-band. With improved fabrication process and device design optimization, Q-factor of PVD AlN on SiO₂-on-Si substrate can be further stretched above 1 million. Considering AlN material having inherent second-order nonlinearity and large bandgap and additional benefits of having AlN on SiO₂-on-Si, such as lower substrate cost and ease of handling, scalability and monolithic integration, AlN on SiO₂-on-Si substrates is a promising platform for realizing integrated photonics circuits for quantum and nonlinear applications from UV to mid-IR.

5. Acknowledgements

We acknowledge the funding support from Agency for Science, Technology and Research (C210917001 (#21709) and C220415015).

6. References

- [1] D. K. T. Ng, G. Wu, T. -T. Zhang, L. Xu, J. Sun, W. -W. Chung, H. Cai, Q. Zhang, and N. Singh, "Considerations for an 8-inch wafer-level CMOS compatible AlN pyroelectric 5-14 μm wavelength IR detector towards miniature integrated photonics gas sensors," *J. Microelectromechanical Syst.* **29** (5), 1199-1207 (2020).
- [2] D. K. T. Ng, L. Xu, Y. H. Fu, W. Chen, C. P. Ho, J. S. Goh, W. W. Chung, N. Jaafar, Q. Zhang, and L. Y. T. Lee, "CMOS AlN and ScAlN pyroelectric detectors with optical enhancement for detection of CO₂ and CH₄ gases," *Adv. Electron. Mater.* **9**, 2300256 (2023).
- [3] C. Xiong, W. H. P. Pernice, X. Sun, C. Schuck, K. Y. Fong, and H. X. Tang, "Aluminum nitride as a new material for chip-scale optomechanics and nonlinear optics," *New J. Phys.* **14**, 095014 (2012).
- [4] C. Xiong, W. H. P. Pernice, and H. X. Tang, "Low-loss, silicon integrated, aluminum nitride photonic circuits and their use for electro-optic signal processing," *Nano Lett.* **12**, 3562-3568 (2012).
- [5] P. T. Lin, H. Jung, L. C. Kimerling, A. Agarwal, and H. X. Tang, "Low-loss aluminium nitride thin film for mid-infrared microphotonics," *Laser & Photonics Rev.* **8** (2), L23-L28 (2014).
- [6] M. Stegmaier, J. Ebert, J. M. Meckbach, K. Ilin, M. Siegel, and W. H. P. Pernice, "Aluminum nitride nanophotonic circuits operating at ultraviolet wavelengths," *Appl. Phys. Lett.* **104**, 091108 (2014).
- [7] X. Liu, A. W. Bruch, Z. Gong, J. Lu, J. B. Surya, L. Zhang, J. Wang, J. Yan, and H. X. Tang, "Ultra-high-Q UV microring resonators based on a single-crystalline AlN platform," *Optica* **5** (10), 1279 (2018).
- [8] X. Liu, C. Sun, B. Xiong, L. Wang, J. Wang, Y. Han, Z. Hao, H. Li, Y. Luo, J. Yan, T. Wei, Y. Zhang, and J. Wang, "Integrated high-Q crystalline AlN microresonators for broadband Kerr and Raman Frequency combs," *ACS Photonics* **5**, 1943-1950 (2018).
- [9] J. Liu, H. Weng, A. A. Afridi, J. Li, J. Dai, X. Ma, H. Long, Y. Zhang, Qiaoyin Lu, John F. Donegan, and Weihua Guo, "Photolithography allows high-Q AlN microresonators for near octave-spanning frequency comb and harmonic generation", *Opt. Express* **28** (13), 19270 (2020).
- [10] X. Liu, Z. Gong, A. W. Bruch, J. B. Surya, J. Lu, and H. X. Tang, "Aluminum nitride nanophotonics for beyond octave soliton microcomb generation and self-referencing", *Nat. Commun.* **12**, 5428 (2021).
- [11] H. Jung and H. X. Tang, "Aluminum nitride as nonlinear optical material for on-chip frequency comb generation and frequency conversion," *Nanophotonics* **5**, 263-271 (2016).